A B S T R A C T

1. Introduction

The study area is situated in the north-eastern part of the Bohemian Massif and comprises the Czech portion of the Sudetic Marginal Fault zone (SMF). The SMF represents one of the most prominent tectonic zones in central Europe. The fault is more than 200-km long and controls the pronounced morphotectonic escarpment of the Sudetic Mountains front for a distance of 130 km (Fig. 1).

Despite the topographic expression of the morphotectonic escarpment (Fig. 2), no historic earthquake event is considered to have been of sufficient magnitude to have generated relief within the Sudetic Mountains. Paleoseismological studies demonstrate that in order to generate a topographic expression, an earthquake event must have a moment magnitude in excess of M 5 (e.g. McCalpin, 2009). By contrast, local historic earthquake intensities have been estimated to reach only $I_0 = 4$–7 MSK (Guterch and Lewandowska-Marciniak, 2002). In order to discover whether prehistoric faulting has indeed been responsible for generating the morphology of the mountain front, a near-fault investigation was undertaken from exposures seen within artificially dug trenches (Fig. 3).

As the region belongs to an intraplate area of central Europe, only low to moderate seismicity would be anticipated (see panel discussion in Mohammadioun, 1995), although also evidence for the occurrence of large earthquakes in such a stable continental regions exist (Camelbeeck and Meghraoui, 1996, 1998). Moreover, the climate and exodynamic processes in the studied area during Pleistocene has not favored good preservation of a fault scarp neither depositional bodies related to an earthquake, since mass wasting during cold periods removed all older Quaternary deposits from steep slopes along the SMF. We have a good control of removal of Pleistocene sediments from this area which were deposited by continental glaciation and covered wider area in the middle Pleistocene (e.g. Prosová, 1981; Sikorová et al., 2006); but
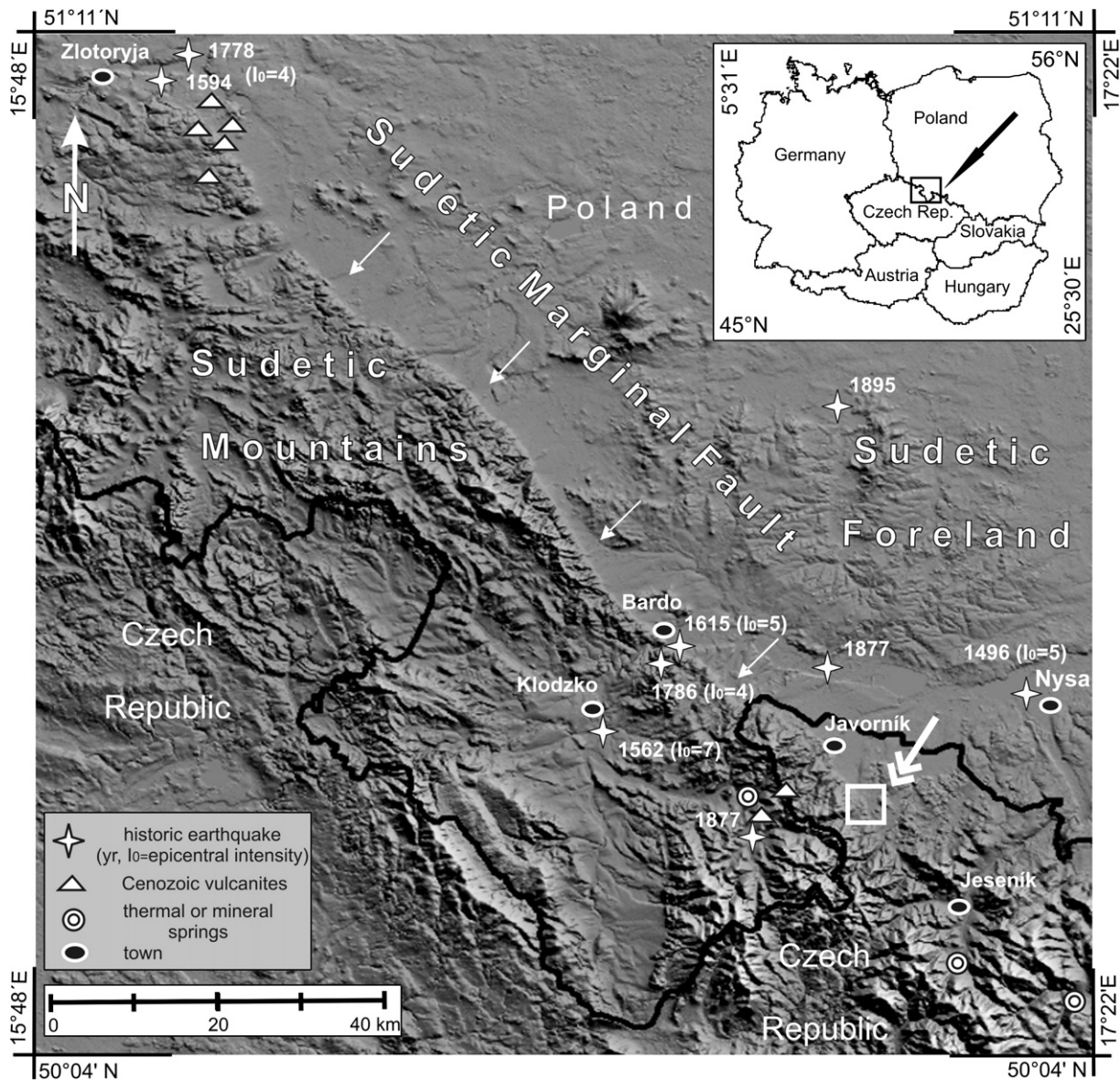
Fig. 1. Topographic situation of the morphologically well-pronounced Sudetic Marginal Fault that divides the Sudetic Mountains from the Sudetic Foreland (SRTM, 90 m resolution). Data on historic earthquakes compiled by Kárník et al. (1958); Olczak (1962); Pagaczewski (1972); and Guterch and Lewandowska-Marciniak (2002). Study area marked by white double arrow.

glacigenic sediments are mostly preserved on flat low-lying areas NE of the fault, with only relic patches in the Rychlebské hory (Mts.) SW of the SMF (Žáček et al., 1995, Pecina et al., 2005). In addition, the fully vegetated area along the SMF lacks outcrops of the fault. Thus, excavating artificial trenches was thought to be the most appropriate method with which to study the SMF in detail.

This elaborate trenching technique has not hitherto been applied on either this particular fault system or elsewhere in central Europe (Štěpančíková and Hók, 2009; Štěpančíková et al., 2009). A detailed study such as this contributes to the definition of fault characteristics, the sense of movement, the history of faulting, and the fault slip rate. Moreover, estimating the magnitude and frequency of paleoearthquakes related to a single slip event has a special importance for hazard assessment in highly populated areas (Petley, 1998). It is therefore pertinent to note that dams in the adjacent Paczków Graben have been geodetically monitored and studied in terms of neotectonic and recent crustal movements, which could be a potential hazard for this region (Cacoń and Dyjor, 1995).

2. Geological setting

The north-eastern front of the Rychlebské hory (Mts) is associated with the NW–SE trending SMF, which separates the mountains of the Sudetic Block to the southwest from the Žulovská pahorkatina (hilly land) in the Fore–Sudetic Block to the northeast (Fig. 2). The Sudetic Block is composed of various types of Paleozoic metamorphic and magmatic rocks of the Staré Město Group, Orlice–Śnieżnik Complex, Stronie Śląskie Group, Velké Vrbno Unit, Branná Group, and Keprník Unit; these rocks comprise gneisses, ortogneisses, phyllonites, marbles, mica schists, metagabbros, erlans, amphibolites, and granodiorites (Fig. 4) (Žáček et al., 1995). In contrast, the down-thrown Fore–Sudetic Block is composed of the late-Variscan Žulová granite pluton dated as 304 Ma (Pecina et al., 2005), which represents an apical part of a vast granitic body (Cháb and Žáček, 1994). To the southeast, the metamorphosed Devonian cover of the pluton comprises gneisses, amphibolites, quartzites, and marbles. The adjacent Vidnava Basin, of Neogene age, is a part of Paczków Graben and has been filled with Miocene strata
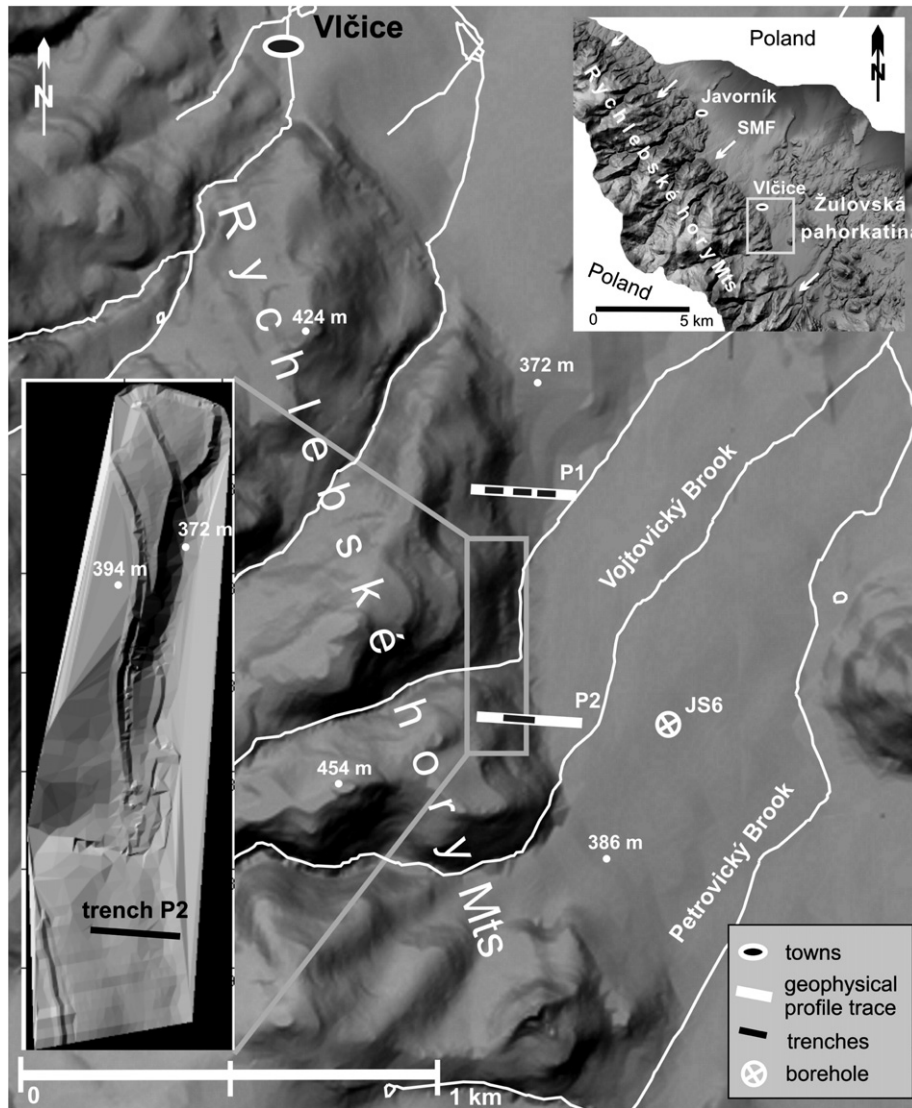
Fig. 2. Localization of the geophysical profiles and trenches on the DEM based on vectorized contour lines of 2 or 5 m interval from 1:10,000 maps. The DEM in the black rectangle on the bottom left is derived from a microtopographic map produced by using a total station. SMF — Sudetic Marginal Fault, JS6 — name of borehole.

reaching up to 680 m thickness; this overlies Early Paleozoic substratum (e.g. Frejková, 1968; Ondra, 1968; Cwojdziński and Jodłowski, 1978; Badura et al., 2004).

Geological maps of the study area near the village of Vlčice u Javorníka show migmatitic gneisses to migmatites with lenses of amphibolites of the Staré Město Group on the Sudetic Block (Žáček et al., 1995; Pecina et al., 2005). In contrast, the adjacent the Fore–Sudetic Block is composed of fluvial to limnic sediments of Miocene age within the Vidnava Basin; these sediments are covered by Quaternary glacial and alluvial deposits. The strike azimuth of the SMF in the vicinity of the study area varies between 132° and 137°, as inferred from the linear trace of the mountain front (Fig. 2). However, in the investigated locality the SE portion of the mountain front starts to change its orientation to N–S. The fault scarp here is more dissected and composed of short echelon sections (Skácel, 1989; Ivan, 1997).

The origin of the SMF and of parallel faults in the area probably pre-dates the early Variscan and since Permian the SMF has experienced alternating vertical movements (Pouba and Mísař 1961; Skácel, 2004). During the Alpine cycle it became reactivated (Badura et al., 2003). Generally, the SMF is assumed to be a normal, steeply-dipping, fault (Oberc, 1977), although also a horizontal component has been documented (Mastalerz and Wojewoda, 1993,

Skácel 2004) Despite the fact that the SMF is a very pronounced structure and its neotectonic activity has been studied intensively (e.g. Oberc and Dyjor, 1969; Dyjor and Oberc, 1983; Skácel, 1989; Mastalerz and Wojewoda, 1993; Dyjor, 1993, 1995; Krzyszkowski and Pijet, 1993; Migoń, 1993; Krzyszkowski et al., 1995, 2000; Ivan 1997; Krzyszkowski and Bowman, 1997; Badura et al., 2003, 2007; Štěpančíková et al., 2008), a comprehensive neotectonic fault history has not been fully elucidated so far. According to Badura et al. (2007), morphometric characteristics of the SMF such as triangular facets appear to confirm the normal character of the fault. However, study of fractured pebbles of Late Pleistocene fluvial sediments within the SMF suggests a dextral component of movement (Badura et al., 2007). Moreover, studies of present-day tectonic activity of the SMF infer diverse present-day stress regimes. SSW–NNE to SSE–NNW compressive stress field was inferred from monitoring of micro-displacements within the SMF using a TM71 deformeter (Štěpančíková et al., 2008). This stress orientation would require a minor dextral component of motion along the SMF. It is in agreement with the borehole breakout analysis carried out in the adjacent area of Fore–Sudetic Monocline, where SSW–NNE maximum horizontal stress is indicated (Jarosiński, 2005, 2006). Although the GPS measurements on the Polish SMF portion show also maximum compression within Sudeten and Fore–

Fig. 3. Picture showing topography of the fault scarp with the position of the Trench P2.

Sudetic Block SW–NE, motion has a possible sinistral component (Kontny, 2003, 2004, Badura et al., 2007). Also GPS data on the Czech portion of the SMF indicate sinistral movements (Nováková and Schenk, 2008; Nováková, 2009).

Despite the morphological expression of the SMF-related mountain front, epicentral intensity of recorded local historic earthquakes was estimated to reach only $I_0 = 4$–7 (MSK) (Guterch and Lewandowska-Marciniak, 2002). The historic earthquakes that were located very close to the fault include those near Zlotoryja/Legnica in 1594 and 1778, and those near Bardo/Dzierżoniźów in 1615 and 1786. Other historic earthquakes that might have been associated with the fault or were felt in the zone parallel to the SMF (Fig. 1) include events in 1496, 1562, 1786, 1823, 1877, and 1895 (Kárník et al., 1958; Olczak, 1962; Pagaczewski, 1972; Guterch and Lewandowska-Marciniak, 2002).

3. Methods

The presented data are the results of fieldwork, which has focused predominantly on trenching across the SMF. First, a digital elevation model (DEM) of the study area was obtained through the ZABAGED project and analysed in detail; this DEM has been constructed from vectorized base maps at a scale of 1:10,000 and with a contour interval of 2–5 m. This DEM analysis was complemented by geomorphological field investigation, which enabled a suitable locality for trenching to be selected. As a result, the N–S striking trace of the SMF that flanks the foot of the mountains of Rychlebské hory, to the south of the village of Vlčice u Javorníka, was selected for further analysis.

Geophysical research was carried out in order to specify the sites to be trenched. Two profiles that crossed the SMF, P1 (length: 255 m; azimuth: 89°) and P2 (length: 343 m; azimuth: 87°), were selected for multi-electrode resistivity (resistivity tomography) and Ground Penetrating Radar (GPR) survey (Fig. 2). The Resistar RS-100M equipment with multi-electrode system ME-100 (Geofyzika a.s. Brno) were used for a multi-electrode survey with a configuration of Wenner→Schlumberger and electrode spacing of 1 m. Primary data were processed by a 2-D inverse method using the program Res2DInv (Loke and Barker, 1995) into resistivity cross sections. GPR measurements were carried out by means of equipment RAMAC X3M with antenna system 250 and 500 MHz (ABEM, Sweden); these data were elaborated by the ReflexW program into the form of time

sections or re-counted depth sections. Only the results determined for Profile P2 are discussed in this study.

Moreover, detailed topographic profiles along the trenches were constructed by means of laser range finder, whilst the area between Profiles P1 and P2 was surveyed using a total station in order to produce an additional microtopographic map (Fig. 2).

Four trenches within the fault zone were dug. Three of the trenches traced Profile P1 for lengths of 10–15 m, whereas the fourth traced Profile P2 for a length of 110 m; this trench had a depth of 2.5 m and a width 1.2 m. Only the latter was furnished by 0.5 m×0.5 m net and documented in detail, due to both the technical and safety constraints afforded by a high groundwater level and the importance of the findings (Fig. 3). The succession of sedimentary units was described and their sedimentary environmental and stratigraphic interpretation is given below. A variety of analyses was undertaken on the samples collected from the trenches, including palynological and clay mineral analysis. Moreover, radiocarbon dating of charcoal and buried soils was performed in laboratories in Gliwice and Poznań (Poland). The IntCAL04 calibration set (Reimer et al., 2004) was used in order to calibrate of radiocarbon data; all the radiocarbon dates presented here are calibrated ages in years before present (cal yr BP), where 'present' is conventionally defined as year 1950 AD.

4. Results

4.1. Geophysics

The results of the geophysical research were interpreted in two stages. The preliminary interpretation aimed to find the optimal position for the trenches; this was executed immediately after surveying, based on general petrophysical knowledge. The SMF was initially identified on Profile P2, between Stations 85 and 138 (the name of stations indicates metrical distance within the profile); this area was characterized by conductive bedrock, with several extremely conductive structures and the occurrence of a spring (Fig. 5). The segment between Stations 78 and 149 was selected for trenching. The final interpretation (reinterpretation) resulted from the comparison of the geophysical data with a detailed lithostratigraphic and tectonic description of geology recorded in the Trench P2, and allowed to infer more information on physical manifestations of the recorded tectonic structures.
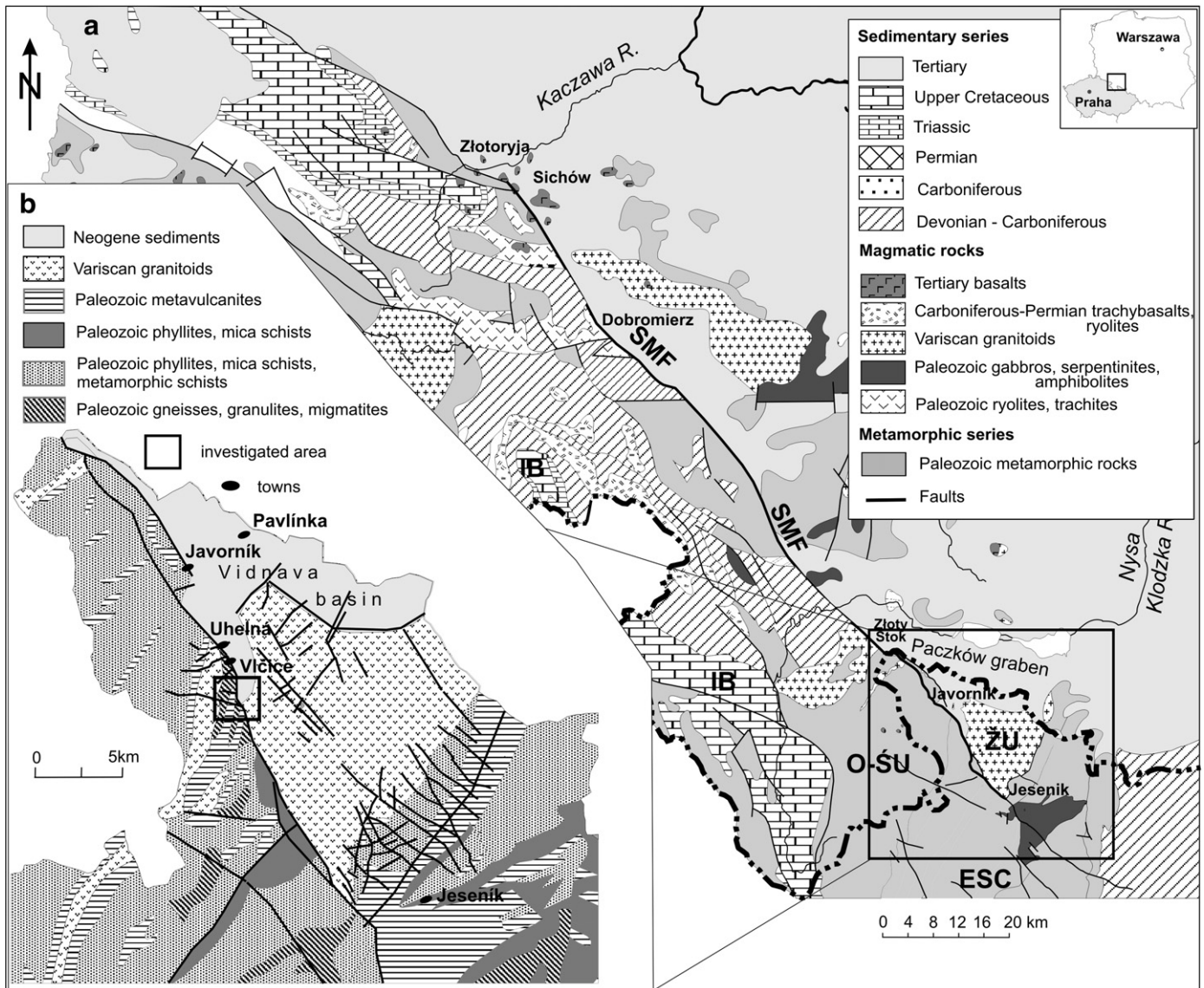
Fig. 4. a) Geological setting of the Sudetic Marginal Fault (SMF) zone modified from Badura et al. (2007): IB — Intra-Sudetic Basin, O-ŚU — Orlice-Śnieżnik Unit, ŽU — Žulová massif, ESC — East Sudetes Complex, and SMF — Sudetic Marginal Fault; b) geological setting of the study area (compiled with the basic geological map by the Czech Geological Survey, 1998).

The shallow part of the section up to Station 120 is characterized by a surface layer of relatively high resistivity (50 to 400 ohm m) and low reflectivity in GPR images; this layer represents Quaternary sandy silts with gravel clasts (Member H; Fig. 6), and reaches depths of 1 to 1.5 m (Fig. 5). Intermediate resistivity medium (50 to 200 ohm m), which manifested itself in greater depth from the start of the profile up to Station 83, is associated with crystalline lithologies (Member F); these rocks are faulted in the east. Underlying material in the section between Stations 83 and 138 is characterized by low resistivities (10 to 50 ohm m), which provides evidence for a sequence of fine-grained Neogene sediments (Members A, B, C); several narrow sub-vertical high conductive structures are distinct. The first part of this sedimentary sequence (between Stations 83 and 102) consists of clayey-silty sands (Member A); within this sequence, localized zones of extreme conductivity are associated with several graphite layers. The second part of the sequence (between Stations 102 and 116) consists of diamict with disintegrated clasts of crystalline rocks; this sequence is characterized by higher conductivity. The third part (between Stations 116 and 138) consists of conductive uncovered kaolinized silty sands. The absence of both the non-conductive layer at the surface and the occurrence of markedly low bedrock resistivities characterize this section; these observations can be explained in part

by high water saturation of sediments (i.e. in the vicinity of the spring, between Stations 125 and 135) and in part by the occurrence of a proposed fault zone in the vicinity of Station 128 (see Section 4.3). The sub-horizontal boundary between higher and lower resistivities situated at a depth approximately 1 m (between Stations 85 and 120) could be likewise caused by borderline between less and more water-saturated rock media.

Close to the surface at the base of the slope (between Stations 139 and 145), the resistivity minimum corresponds to the layer of recent sandy silts with gravel clasts. The remainder of the profile (between Stations 142 and 400) is characterized by the presence of a layer that is associated with high to extremely high resistivities and high GPR reflectivity and is situated underneath the thin superficial layer. It corresponds to muddy gravels within a Pleistocene alluvial fan. The zones of resistivity maxima indicate that these areas are dominated by cobble material with only a minor fine-grained content. The thickness of the non-conductive layer varies from 3.5 to 7 m; these depths are similar to that found in a nearby borehole, where the thickness of Late Pleistocene alluvial fan deposits were documented to be about 9 m (Skácel, 1978). The localized depressions at the base of the deposit might indicate paleochannels within the alluvial fan, even where accompanied by high resistivities; these depressions are particularly
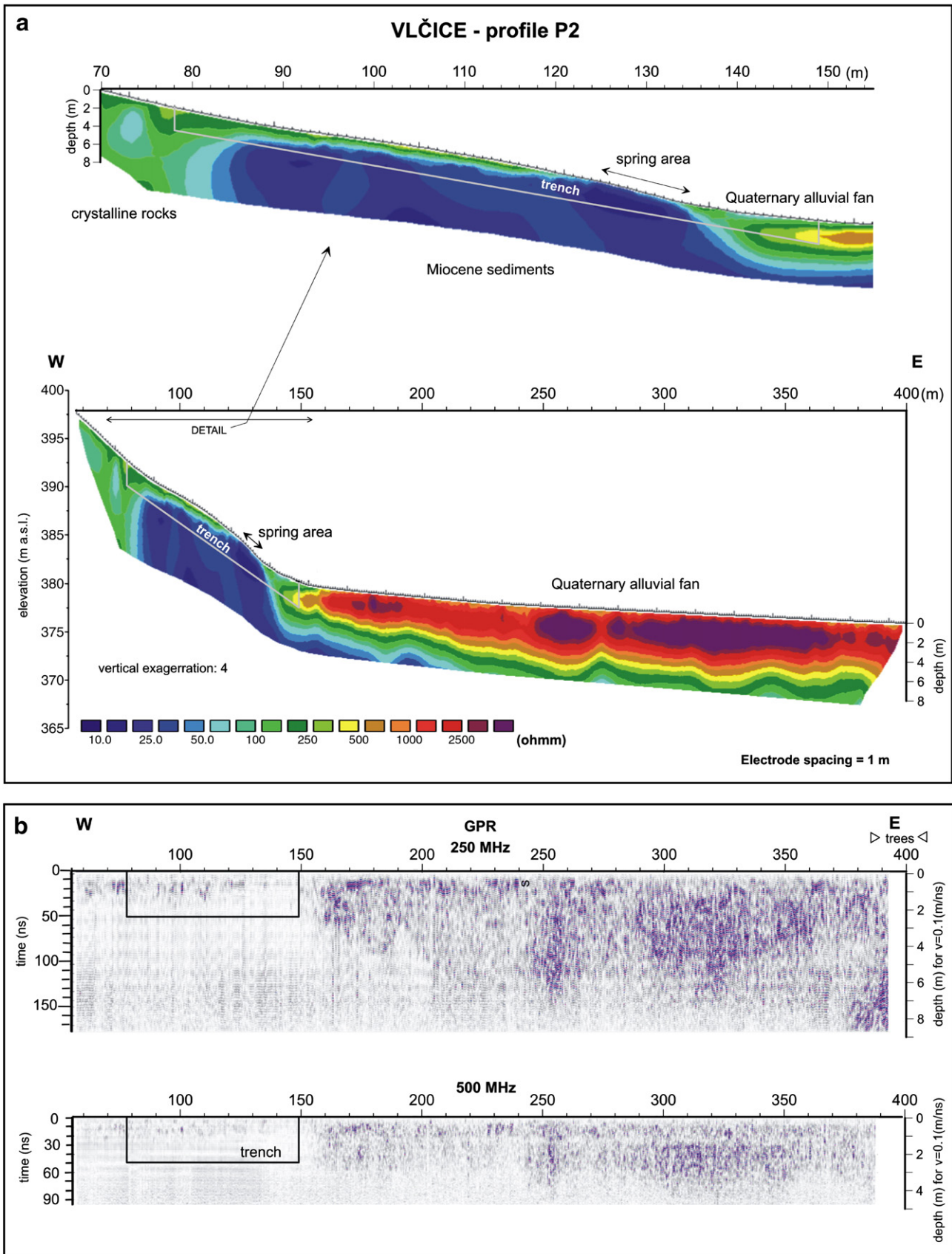
Fig. 5. Results of geophysical sounding at the Profile P2: a) Multi-electrode resistivity survey (resistivity tomography); and b) Ground Penetrating Radar (GPR) survey; black line shows the position of the Trench P2. For interpretation see the text in Section 4.1; the distance in meters corresponds with the name of stations in the text.
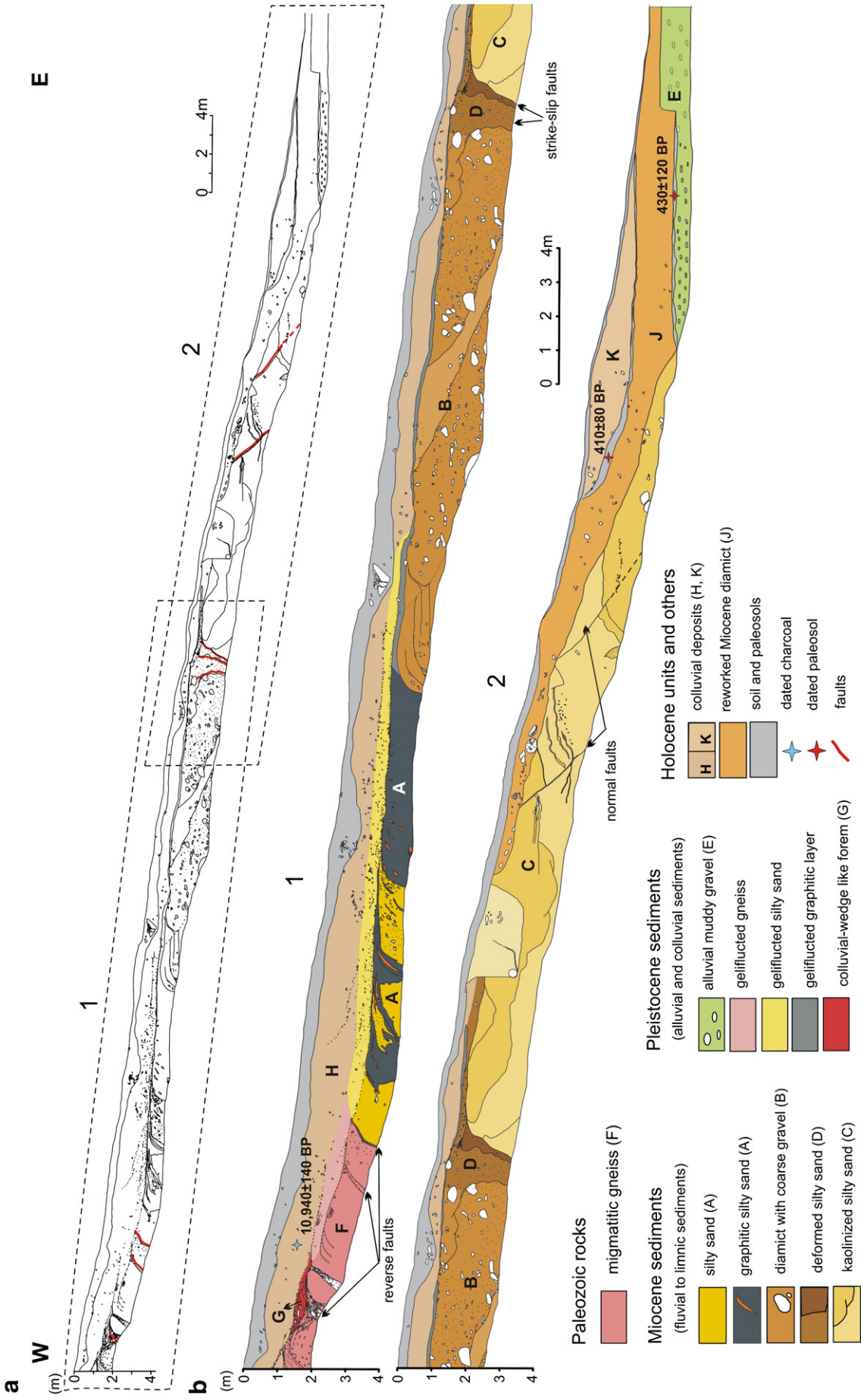
Fig. 6. Log of the Trench P2 in Vlčice site, unexaggerated: a) Overall log of the southern wall; and b) two parts 1 and 2 of the log with geological information.

notable in the vicinity of Station 258 and between Stations 320 and 330. They are also recognizable in the GPR-section around Stations 255 and 320. Beneath the high resistivity layer, there are comparatively more conductive rocks (below GPR penetration depth), which probably represent clayey-sandy Neogene sediments. The reflexes recorded by the GPR at depths of more than 4 m in the vicinity of Station 390 are air reflexions from trees alongside the Vojtovický Brook (imperfectly shielded antenna).

4.2. Sedimentary units

Trenching across the SMF revealed a succession of sedimentary units (Fig. 6). These are briefly described for Trench P2, along with their environmental and stratigraphic interpretation.

The Neogene sequence comprises disturbed beds with three different members, which have been informally termed A, B, and C. The uppermost of these, Member A, is characterized by an alternation of dark greyish silty sands and rusty silty sands; the dark greyish layers contain abundant graphite. In the middle, Member B is characterized by a matrix-supported diamict with abundant, completely disintegrated, clasts of amphibolites, gneisses and migmatites that are up to 25 cm in diameter. Beneath this, Members B and C are separated by a ~1 m thick "deformation" zone (D), which corresponds to a fault. The lowermost of these, Member C, is characterized by kaolinized silty sands with gravel clasts of disintegrated granites, amphibolites, and rarely gneisses. In some places, gravel sand layers with distinct planar or low-angle tabular cross-bedding are included.

All the described members correspond to the sedimentary units logged from boreholes drilled in the Uhelná deposit, i.e. in the central part of the western part of the Vidnava Basin, which is filled primarily by fluvial to limnic sediments, and that extends from Vlčice across Uhelná to Pavlínka further north (Fig. 4). However, sediments of Member A have been overturned and disturbed to a nearly vertical position and sediments of Members B and C have been tilted in Trench P2. Both Members A and C were deposited in a fluvial to fluvio-limnic environment within the tectonically active basin periphery. Member B represents debris-flow deposits deposited along the active basin margin. These sediments are stratigraphically classified, according to pollen and plant macro-remains, to the Carpatian to lower Badenian (i.e. early to mid Miocene, ~18–15 Ma, Gabriel et al., 1982).

The uppermost parts of Members A and B have been reworked in to layers of up to 20 cm by sheet gelifluction (Fig. 6). This gelifluction was very probably associated with the seasonal thawing of the uppermost part of the active permafrost layer, at a time when there was only sparse vegetation; under such conditions, the uppermost unconsolidated material behaves plastically and is slowly displaced down-slope. The specific process of gelifluction, opposed to the more general process of solifluction, is invoked to explain the displacement of materials because of the specifically layered nature and typical downward displacement reduction of these reworked materials, despite minor frost upheaval traces that may reflect diurnal frost creeping associated with ice lensing; solifluction is currently invoked to comprise a wide-range of superficial movement processes from frost-creep to plug-like flow (Matsuoka, 2001; French, 2007). Gelifluction is associated with frozen ground permafrost conditions, seasonal thawing, and one-sided freezing of the active layer; therefore, the latest time that these processes could have occurred was before the dramatic warming of the Younger Dryas/Preboreal at the beginning of the Holocene.

Alluvial muddy gravels are deposited at the base of the slope (Member E). These gravels are here described as ranging from intermediate to sandy diamicts, through to conglomerates with a sandy- to silty-matrix and a large proportion (~30%) of gravel clasts that are mostly up to 20 cm (max. 65 cm) in diameter. These sediments are very poorly to extremely poorly sorted, and a matrix-supported structure prevails. Imbrication is poorly visible, although horizontally laid discoidal clasts are common where clast-supported structure is apparent. Gravel clasts are typically sub-angular to sub-rounded; these clasts are composed of migmatites, amphibolites, gneisses, and phyllites, with less common quartz and granite. The matrix contains a high proportion of micas, which may be the result of post-depositional mechanical and chemical weathering. A number of notable more sorted sandy layers or lenses up to 40 cm thick and <2 m long are present. The thickness of the alluvial sediments in boreholes hereabouts ranges between 6 and 9 m (Skácel, 1978; Pecina et al., 2005). These alluvial sediments represent the youngest phase of alluvial deposition in region; deposition either took place during the kataglacial phase of the last (Weichselian) glaciation, or possibly even during the Late Glacial as it is not covered by pleniglacial loess that covers the older surfaces in the region. The channel cut into their surface (see Fig. 6) displays a sharp erosional base that had probably already developed prior to the final phase of alluvial fan deposition at the base of the hill; this is evidenced by marked erosional incision into the alluvial fan surface. This channel was initially used by Vojtovický Brook, before it was diverted by human agricultural activities; distinct medium-sorted fluvial coarse-grained sands to granules within lenses of <40 cm are capped by a fluvisol dated at 430 ± 120 cal yrs BP, which demonstrates the NW flow of Vojtovický Brook along this channel up to early modern times.

Member G, in the upper part of the slope, comprises colluvial sediments deposited in a wedge-like form overlaying a parallel reverse fault. It consists of unsorted sandy silts with gravel clasts of the crystalline rocks derived from hanging wall.

The lower part of colluvial sediments (Member H) in the upper part of the slope are represented by sandy silts with some (2–5%) gravel clasts up to 5 cm in diameter, and with a variable thickness of between 0.5 and 1.5 m. The sediments are poorly to very poorly sorted; they are mottled, contain sub-vertical infiltrations along fissures, and bear traces of distinctive gleysation. The gravel clasts are mostly sub-rounded to sub-angular and consist of migmatites, amphibolites and gneisses. Their poor sorting and lack of layering show that the process of transportation was not associated with freezing and thawing, but more probably with water saturation; such conditions were more likely during the Holocene. This timing has subsequently been confirmed by the radiocarbon dating of charcoals taken from the middle part of these colluvial sediments, which has recorded an age of $10,940 \pm 140$ cal yrs BP. It is thought that deposition continued throughout the Holocene.

Colluvial sediments at the base of the hillslope (Members J and K) comprise homogeneous sandy silts with some gravel clasts (~5%) up to 15 cm in diameter. These colluvial sediments contain a high proportion of material clearly originating from the debris-flow deposits of Member B (see above). The sequence formed by Members J and K is characterized by an undulating erosional base, without obvious bedding; these sediments are poorly to very poorly sorted, with mostly sub-rounded and less sub-angular clasts. The maximum sedimentary thickness reaches ~2 m at the base of the hill, although it is generally between 0.5 and 1.5 m. The deposition of this unit was a result of the slow sheet-like frost creeping of the uppermost regolith mantle. It also contains a buried horizon of soil sediments of luvisol type at the base of the hill, which is covered by ~60 cm of slightly finer colluvial sediments; this buried soil sediment was dated at 410 ± 80 cal yrs BP and its burial may be associated with enhanced anthropogenic activity, as widespread deforestation and extensive agricultural use of the landscape characterized the post-colonial period from the 15th to early 17th century.

4.3. Structural data

In agreement with the geophysical data, the major fault that separates the crystalline rocks of the Sudetic Block (including the Rychlebské hory) and the Miocene sediments overlying crystalline rocks of the Fore–Sudetic Block (including the Žulovská pahorkatina) has been exposed in the trenches. In contrast to previously published geological maps (e.g. Žáček et al., 1995, Pecina et al., 2005), this
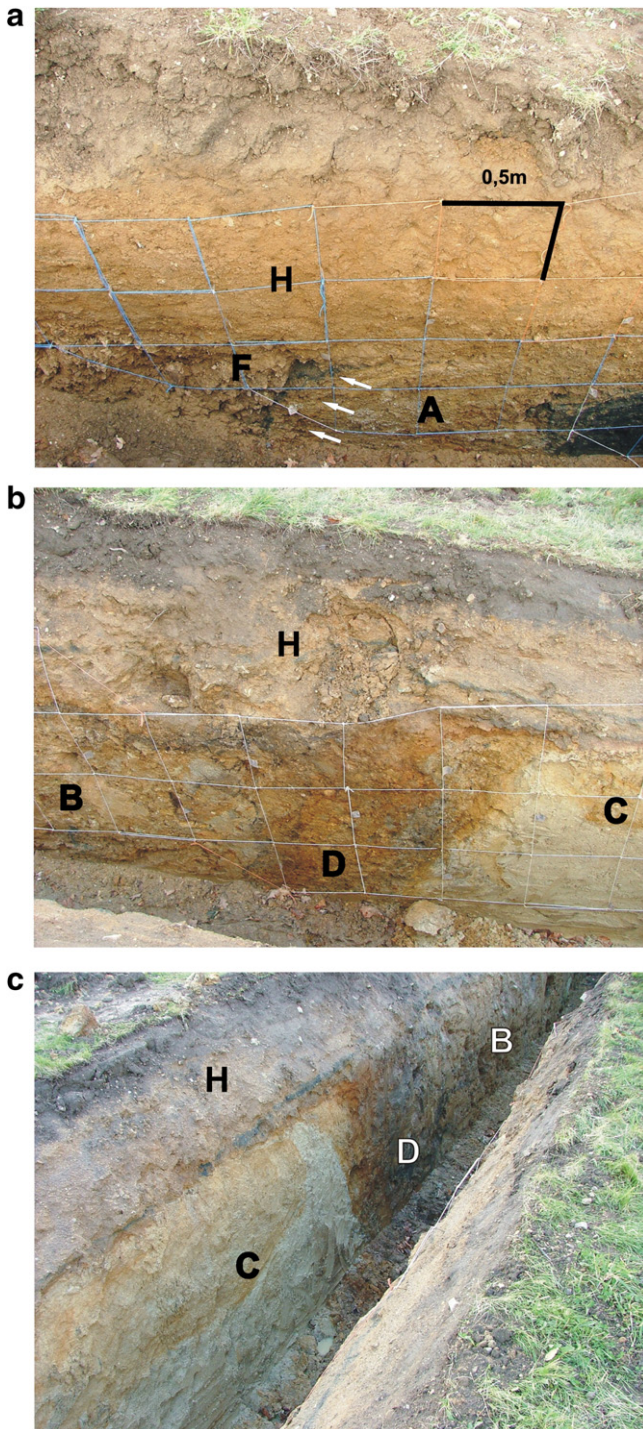
Fig. 7. Pictures of the Trench P2: a) Reverse fault contact between crystalline rocks and Miocene sediments pointed by white arrows; b) deformation zone of probably strike-slip fault character with a feature of flower structure, note dragged unit C; and c) the same as in b but at the opposite western wall; A, B, C — Miocene sediments, A — silty sands silts, B — matrix-supported diamict, C — kaolinized silty sands, D — deformation zone of probably strike-slip faults, F — crushed crystalline rocks, and H — early Holocene colluvial deposits.

important geological boundary does not trace the foot of the mountains but is instead located further upslope. The fault has been identified as a reverse displacement of crystalline rocks over Miocene deposits, accompanied by a 2–4 cm thick layer of graphite (Fig. 7a). The strike azimuth of this reverse fault is 160° (i.e. in the Sudetic direction), with dips of between 40 and 70° to WSW (Fig. 8). Moreover, myllonites with S–C structures (sensu Lister and Snoke,

1984) were identified at the contact within the crystalline rocks; they indicate that the fault zone hereabouts must have experienced reverse oblique displacement with sinistral component most probably during the ductile Variscan deformation of the crystalline complex. The contact between crystalline rocks and Miocene deposits was exposed also in the uppermost trench within Profile P1, and a similar strike azimuth (155°) was recorded. However, these two sites are disconnected, which implies an en echelon structure, or that the fault splays or that a younger transversal fault displaces the fault line.

A further minor reverse fault has also been identified within the crystalline rocks. It includes a pegmatite dyke and divides more compact crystalline rocks from a zone of crushed rocks. This fault created a step in the relief, which has been subsequently covered by colluvial sediments; in the trench, the step appears to be 0.6 m high for a distance of 1.3 m (Fig. 6). The colluvial sediments (Member H) were dated as $10{,}940 \pm 140$ cal yrs BP, based on an inclusion of charcoal. As the step must have been at surface before the deposition of these early Holocene sediments, the movement along this fault has probably occurred as recently as the Late Pleistocene. If this movement had been slow, a step of this size would have been completely obliterated by subsequent erosion; as the step is still recognizable beneath Holocene sediments, it seems that the movements were sudden and it is here proposed that the origin of this step probably relates to an earthquake event. A seismic origin is also suggested by a depositional form (Member G), which appears to be analogous to a colluvial wedge; a depositional form such as this is considered to be typical for sudden (seismic) movements (Fig. 6) (McCalpin, 2009). Above the reverse fault, this form has not been affected by gelifluction and therefore movement along this fault must have occurred after Late Glacial gelifluction but before $10{,}940 \pm 140$ cal yrs BP.

In the middle part of the trench, a deformation structure (D) separates Members B and C; this structure is a 1 to 1.5 m wide sub-vertical zone, with strike azimuth 35° and a dip 75° to ESE (Fig. 8). Layers of Member C are dragged upwards along the eastern side of the structure (Fig. 7b, c), which is similar in cross-section to structures observed on strike-slip faults with a certain vertical component (e.g. Moreno et al., 2007). Here, the margin of the plastic silty sands is undulating and interfused with material of the fault zone. If it is assumed that movements along this particular fault occurred under the same stress regime as the reverse movements described above, the strike-slip component on the fault with strike azimuth 35° would be probably dextral.

In the lower part of the trench, two minor faults with normal offset (22 and 35 cm) within Member C were documented. One of them was filled with a greyish clay, probably a fault gauge, and has strike azimuth 145° (the Sudetic direction) with a dip of 45° to NE (Fig. 8). It is worth noticing that the position of the normal fault within the trench profile coincides with the point at which the erosional and depositional character changes. The gelifluced layers of Miocene sediments (Members A and B) and the early Holocene deposits (Member H) end here. Above this normal fault zone, there is the reworked deposit of Member B, Member J, which has been deposited after 430 ± 120 cal yrs BP. Member J contains a paleosol (410 ± 80 cal yrs BP) and is covered by the youngest colluvium (Member K) with a modern soil. The secondary Holocene redeposition of those Miocene sediments formerly within Member B may relate to reactivation of the normal fault; however, the redistributed material that comprises Member J has probably come from another part of slope, as evident from the slightly different ancient slope aspect documented in the trench. Moreover, the spatial arrangement of the gelifluced layers also suggests a disparate slope angle prior to the Holocene. The previously discussed area with the normal fault coincides with the convex part of the slope, at the point where the sub-horizontal upper part of slope (see the gelifluced layers slope angle) is separated from the steeper lower part (Fig. 6). In addition, a
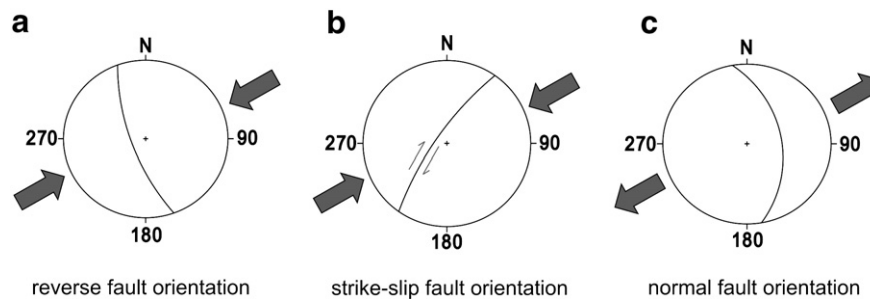
pronounced spring occurs hereabouts, which is also expressed by a very low resistivity (see Fig. 5).

It is also salient to note that the postulated fault that would control the foot of the mountain front has not been identified, as the contact between the Miocene deposits and the Late Pleistocene alluvial fan was too deep to be exposed in the trench.

4.4. Laboratory analyses

In order to determine the age of the sedimentary units within Trench P2, in particular samples including an organic mass were analysed.

Three samples were collected for radiocarbon dating from the Holocene sediments and paleosols. The charcoal exposed in the colluvium (Member H) was determined as *Pinus sylvestris*, with a radiocarbon age of $10,940 \pm 140$ cal yrs BP. Palynological analysis of immature paleosols and soil sediments resting on the Members E and J, has shown presence of an organic mass but no pollen; the former has a radiocarbon age of 430 ± 120 cal yrs BP, whereas the latter has a radiocarbon age of 410 ± 80 cal yrs BP.

In addition, the organic mass from the Miocene sediments (Member A) was analysed. As the particles were resistant to treatment with oxidation agents (e.g. acetolytic mixture and potassium hydroxide), they are not the residue of an organic material such as cellulose or sporopollenin; without any presence of a plant material, the organic mass was shown to be sterile. Further investigation of this organic mass was undertaken through optical microscopy and microphotometry in reflected monochromatic ($\lambda = 546$ nm) and polarized light. Organic petrological investigation has shown that these samples contain various types of highly coalified and graphitized carbonaceous particles differing from each other in morphology and optical properties. The very small (<10 μm), irregular to spine shaped particles (Fig. 9a, b) are abundant in all samples (60–100 vol.%), but are dominant in samples away from the shear-zone contact. Although meaningful maximum and minimum reflectance values are often difficult to obtain due to the extremely small particle size, values of R_{max} range from 4.76% to 7.50% whilst values of R_{min} from 1.88% to 2.44%. These R_{max} and R_{min} values correspond to the vitrinite reflectance values in anthracite and meta-anthracite (Kwiecinska and Petersen, 2004).

The second type of particles has lath-shaped bodies and nodules of well-ordered graphite (Fig. 9a). These nodules may be up to 300 μm, with a very high maximum reflectance ($R_{max} = 11.6$–15.35%) and low minimum reflectance ($R_{min} = 0.78$–1.02%). The number of these particles decreases with the distance from the shear-zone contact.

Reflectance values of carbonaceous particle types correspond with structural characteristics of Raman spectroscopy (Diesel et al., 1978; Suchý et al., 2007; Kříbek et al., 2008). First-order Raman spectra of fine anthracitic and meta-anthracitic particles display a very large D band (Fig. 10a), and thus the ratio of integrated intensities of G (~ 1580 cm^{-1}) and D (~ 1350 cm^{-1}) bands (Tuinistra and Koenig, 1970) is low ($G/D = 1.92$ and 2.65); this indicates a poorly ordered carbonaceous substance. In highly ordered graphite particles, the D band is far smaller (Fig. 10b) and therefore the G/D ratio is high ($G/D = 3.08$–5.26).

The presence of graphite in the Miocene sediments (Member A), documented in the both Trenches P1 and P2, may have resulted from the migration of graphite along the fault zone; this possibility is suggested as graphitized rocks (e.g. shales, gneisses, phyllites, and quartzites) occur at several localities within the SMF zone, as well as underlying the Miocene sediments within the Vidnava Basin (Skácel, 1978). However, further work will be needed to definitely constrain the origin of the graphite.

5. Faulting history

The oldest documented movements within the trench are associated with the myllonites, with the S–C structures, identified in the crystalline rocks, formed during ductile deformation of Variscan orogenesis. These are located close to the reverse fault contact, with
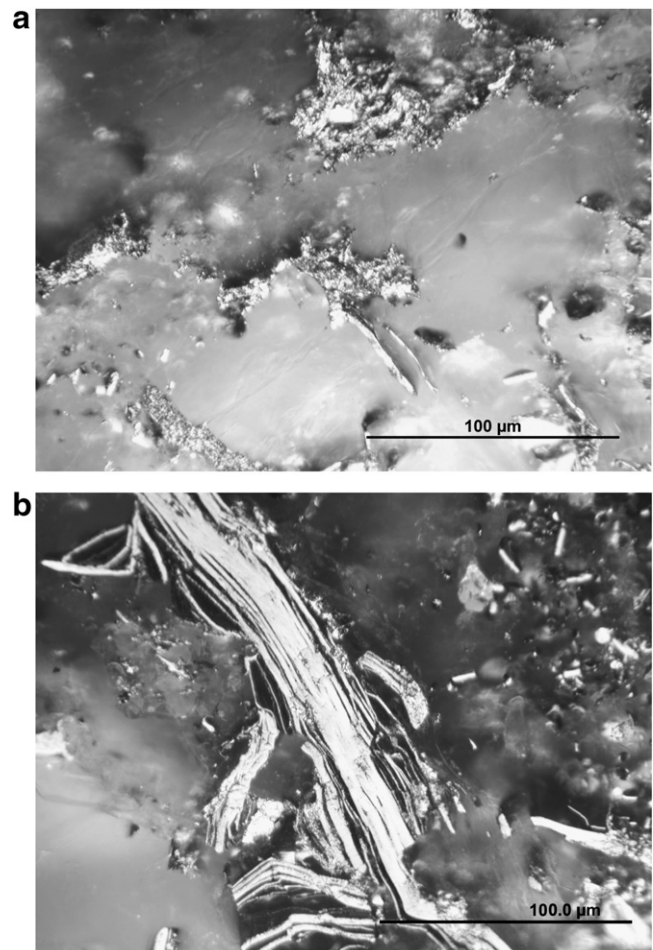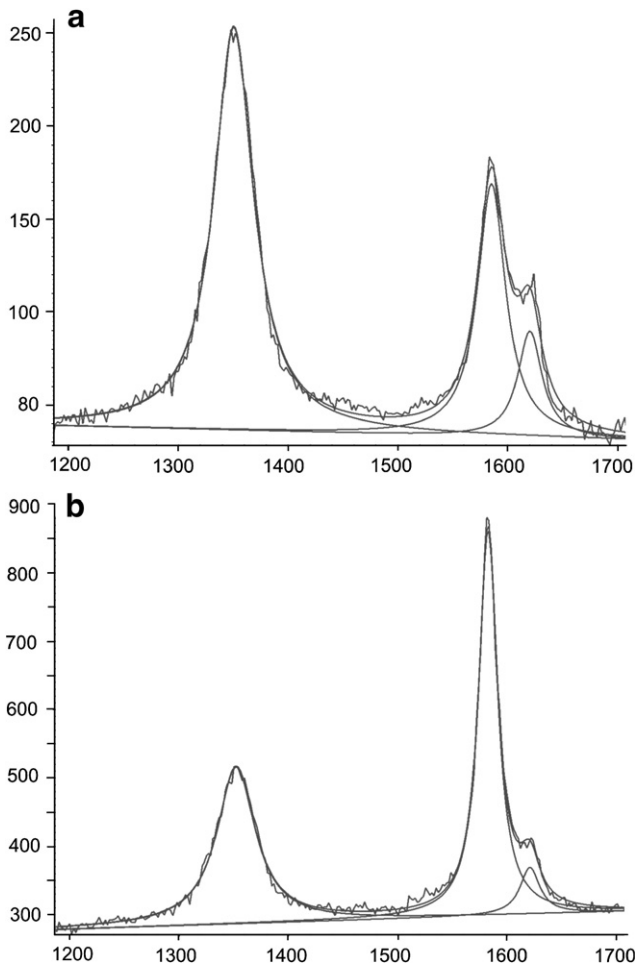

Fig. 9. a) Agglomerates of fine-grained carbonaceous particles and short lath-shaped graphite particles; and b) lath-shaped particles of high ordered graphite.

Fig. 10. Representative Raman spectra with *D* band (~1350 cm^{-1}) and *G* band (~1580 cm^{-1}) of basic types of carbonaceous particles in studied sediments: a) An isotropic small carbonaceous particle with reflectance $R_{max} = 2.15\%$ which suggests an anthracite rank; and b) large particle of high ordered graphite with reflectance $R_{max} = 11.85\%$.

strike azimuth 160°, which separates crystalline rock from Miocene sediment; they indicate reverse oblique displacement with sinistral component.

Thereafter, all identified deformation post-dates the deposition of early to mid Miocene sediments; these have been disturbed and their layers overturned to a near-vertical position or tilted (Fig. 6). When correlating the results from borehole JS6 (Skácel, 1978), which was drilled in the adjacent basin about 400 m from the present study site, it may be suggested that the sediments are no longer *in situ* but have been dragged by the reverse fault (Fig. 11). This supposition is based on the sedimentary sequence encountered in the borehole, where the vertical succession met Quaternary coarse alluvial sediments, Member C, and sediments similar to Members B and A; no graphite-rich layers were noted in the borehole. Moreover, the closer to the reverse fault the more vertically positioned the Miocene layers are. It might be either due to the closeness to the source of deformation or to repeated movements along the contact reverse fault, which deformed more the older Miocene layers. In order to verify the proposed model of dragged layers due to reverse faulting, further drilling close to the fault zone would be required; alternatively, it may be possible to apply other geophysical methods if they are able both to penetrate more deeply and are able to distinguish the course of the deformed individual sedimentary layers.

With regard to the timing of Miocene deformation, the only constraints are provided by the stratigraphic position of the sediments themselves. As movement on the reverse fault has displaced crystalline rocks over Miocene sediments, and as included graphite is covered by gelifluctated layers, this movement must have pre-dated the marked period of gelifluction (Fig. 6). The latest possible time that such gelifluction displacement of this material could have occurred was during Late Glacial conditions, prior to the onset of early Holocene warming. Therefore, the supposed horizontal movement of Miocene sediments in the middle part of the trench along fault zone *D* is thought to post-date the dragging of sediments due to the reverse faulting, but pre-date the Late Glacial gelifluction.

In the upper part of the trench, the reverse faulting identified within the crystalline rocks and the associated colluvial wedge-like form is indicative of sudden, seismic movements. It is covered by the early Holocene colluvium (10,940 ± 140 cal yrs BP) but it is not anymore affected by the sheet gelifluction as the underlying units. It implies its occurrence at the very beginning of the Holocene (Figs. 6 and 11).

The youngest fault movements might have occurred on the lowest part of the slope; these movements may be related to the normal fault that cuts the Miocene sediments. It appears that this fault has been reactivated several times, and that the coinciding documented geodynamic processes (movements and erosional/depositional processes) probably post-date early Holocene colluvial sedimentation (10,940 ± 140 cal yrs BP) but pre-date soil burial (410 ± 80 cal yrs BP); the soil has been buried by the youngest colluvial sediments (Member K) at the base of the slope, possibly in connection with enhanced anthropogenic deforestation and agricultural activity in the early modern times (Fig. 6). Provided that the above mentioned coincidence (see also Section 4.4) of the normal faults and marked change of character and age of overlying depositions, as well as the change of slope angle becoming convex, indicate activity related to the normal faults, the latest movements would occurred between 10,940 ± 140 and 430 ± 120 cal yrs BP. However, these are only indications and no direct evidence of the normal faulting with this time constraint was documented, since the trench exposed only the Miocene sediments to be displaced. Nevertheless, due to different required stress orientation the normal faulting could not have been simultaneous with the older reverse and horizontal movements faulting the Miocene sediments.

Although the presence of the colluvial wedge related to the reverse fault within crystalline rocks is the only direct indication of co-seismic rupture, we can conclude at least about the minimum moment magnitude for the studied segment of the SMF. If we consider the vertical offset inferred from the height of the fault scarp beneath the colluvial wedge 0.3 m as a maximum displacement, according to empirical relationship 'magnitude versus maximum vertical displacement' (Wells and Coppersmith, 1994) estimated minimum is around *M* 6.3. Moreover, a minimum vertical slip rate for this younger reverse fault was estimated basing on the age of the faulted surface and on its vertical offset. As the colluvial wedge post-dates the gelifluctated layers (Late Glacial ~ 15–11 ka) and pre-dates the early Holocene deposits (10,940 ± 140 cal yrs BP), the inferred slip rate is about 0.03 mm/year. It is consistent with slip rate estimation 0.02–0.05 mm/year for Quaternary faults in Poland, which also include the SMF (Zuchiewicz et al., 2007).

6. Final remarks and conclusions

The results of the undertaken geophysical research illustrate that the contact between crystalline rocks and Miocene sediments can be unambiguously identified, as it generates outstanding resistivity discontinuous plane; this boundary is seen even where the crystalline rocks have been tectonically crushed. The identification of individual tectonic faults within the conductive sediments is more ambiguous, and less direct evidence is available. For example, the presence of faults is indicated by secondary graphite enrichment, water-saturated structures, and discontinuous structures filled with clay; all these phenomena lead to decreased rock-medium resistivity, and their manifestation
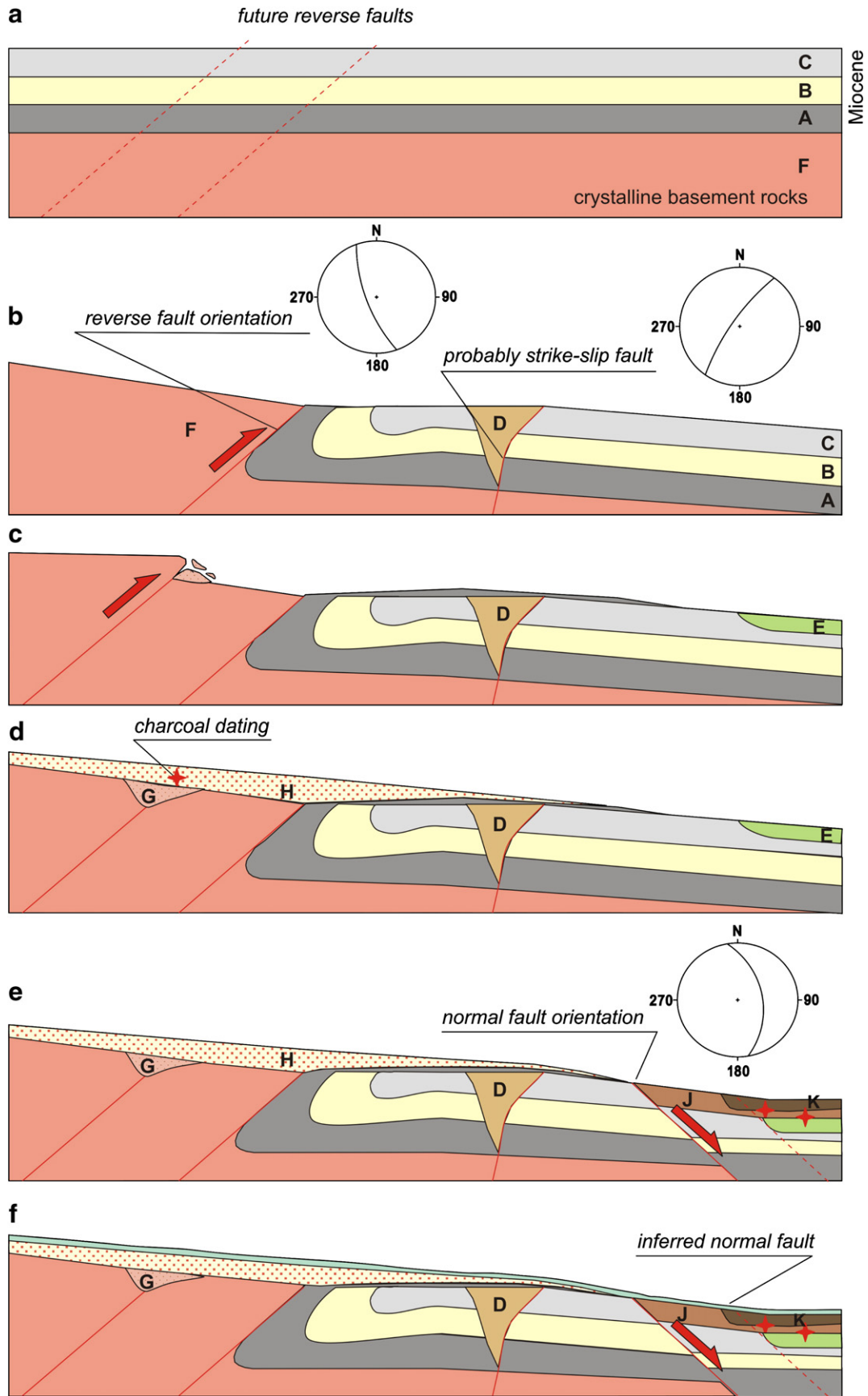
Fig. 11. Retro-deformation series of movements interpreted from the Trench P2. a) initial position of Miocene fluvial to limnic sediment layers (A–C) overlaying crystalline basement (F), b) reverse faulting that dragged Miocene layers and strike-slip movements cutting the sediments, followed by erosion, c) younger reverse faulting that follows deposition of Late Pleistocene alluvial fan (E) and gelifluction of Miocene layers, d) fault scarp erosion and deposition of colluvial wedge (G) followed by deposition of early Holocene colluvial sediments (H), e) (?) normal faulting and possibly related deposition of Member J, followed by deposition of the youngest colluvial sediments (K), and f) present-day situation with recent topsoil.

Table 1

Time constraint of faulting history within the SMF based on the age of deformed sediments, radiocarbon dating of charcoals and paleosols covering the deformed sediments.

Type of deformation	Time limits of movements	
	Maximum	Minimum
Reverse faulting	15 Ma yrs BP	15–11 ka yrs BP
Horizontal movements	15 Ma yrs BP	15–11 ka yrs BP
Reverse faulting	15–11 ka yrs BP	$10,940 \pm 140$ yrs BP
Latest (?) normal faulting	$10,940 \pm 140$ yrs BP (?)	430 ± 120 yrs BP (?)

in the form of local extremely conductive structures serves as an indirect record of fault tectonics. Unfortunately, the applicability of GPR is fundamentally limited by the conductivity of the particular medium being penetrated; as the conductivity of rock increases, the depth to which the radar can penetrate is dramatically reduced.

The trenching technique has proved to be a powerful tool for near-fault investigations in the intraplate region with low slip rate and, moreover, where no fault outcrops are available due to dense vegetation. Although the geomorphological analysis indicated that the SMF is active, further subsurface research was needed to elucidate the character of faulting. At least four general phases of tectonic movements since Miocene within the SMF zone have been documented in the trench; these have been distinguished as a result of the application of dating techniques, as well as through petrological, sedimentological, and structural analyses. The following paragraphs summarize these phases chronologically.

Deformation of the Miocene sediments, which appear to be tilted and overturned up to a near-vertical position due to a reverse fault with strike azimuth 160°, post-dates their deposition but pre-dates Late Glacial gelifluction. The reverse fault displaced crystalline rocks over the Miocene sediments and is filled with a 2–4 cm thick layer of graphite. Inferred horizontal movements along a deformation structure with strike azimuth 35° have the same wide time constraint. Younger reverse faulting, which probably caused the co-seismic step-like relief documented in the trench, post-dates the Late Glacial gelifluction but pre-dates the early Holocene colluvium ($10,940 \pm 140$ cal yrs BP). The youngest activity might be related to a normal fault with strike azimuth 145°, which cuts the youngest Miocene unit; the last reactivation of this fault possibly post-dates early Holocene colluvial sedimentation but pre-dates a buried soil of early modern times (430 ± 120 cal yrs BP). However, the time constraint for this youngest normal faulting is based only on indications and no direct evidence has been documented, thus, they might be much older.

Table 1 summarizes the faulting history. From this, it can be seen that the timing and number of pre-Holocene tectonic movements cannot be constrained with great precision due to the lack of preserved older Pleistocene sediments within the study area; such sediments may themselves have been faulted prior to their subsequent erosion. Despite these difficulties, our data demonstrate Late Quaternary tectonic and seismic activity, which has partly controlled the relief development in the area. At least one prehistoric earthquake has been identified. Respective minimum moment magnitude M 6.3 and slip rate 0.03 mm/year could be estimated. However, the obtained data have not supported the general idea of the SMF to be a sinistral-normal fault and further trenching investigation within other segments of the SMF is desirable.

Acknowledgements

References

Badura, J., Zuchiewicz, W., Górecki, A., Sroka, W., Przybylski, B., Żyszkowska, M., 2003. Morphotectonic properties of the Sudetic Marginal Fault, SW Poland. Acta Montana, Series A 24 (131), 21–49.

Badura, J., Przybylski, B., Zuchiewicz, W., 2004. Cainozoic evolution of Lower Silesia, SW Poland: a new interpretation in the light of Sub-Cainozoic and Sub-Quaternary topography. Acta Geodynamica et Geomaterialia 1 (135), 7–29.

Badura, J., Zuchiewicz, W., Štěpančíková, P., Przybylski, B., Kontny, B., Cacoń, S., 2007. The Sudetic Marginal Fault: a young morphotectonic feature at the NE margin of the Bohemian Massif, Central Europe. Acta Geodynamica et Geomaterialia 4 (148), 7–29.

Cacoń, S., Dyjor, S., 1995. Neotectonic and recent crustal movements as potential hazard to water dams in Lower Silesia, SW Poland. Folia Quaternaria 66, 59–72.

Camelbeeck, T., Meghraoui, M., 1996. Large earthquakes in northern Europe more likely than once though, Eos, Transactions American Geophysical Union 77 (42), 405–409.

Camelbeeck, T., Meghraoui, M., 1998. Geological and geophysical evidence for large palaeo-earthquakes with surface faulting in the Roer Graben (northwest Europe). Geophysical Journal International 132, 347–362.

Cháb, J., Žáček, V., 1994. Geology of the Žulová pluton mantle (Bohemian Massif, Central Europe). Bulletin of the Czech Geological Survey 69, 1–12.

Cwojdziński, S., Jodłowski, S., 1978. Ukształtowanie powierzchni podłoża I geologia kenozoiku południowo-wschodniej części bloku przedsudeckiego. Kwartalnik Geologiczny 22, 181–193.

Czech Geological Survey, 1998. Digital Geoatlas of the Czech Republic 1:500 000, GEOCR 500. Prague.

Diesel, C.F.K., Brother, R.N., Black, P.N., 1978. Coalification and graphitization in high-pressure schists in New Caledonia. Contributions to Mineralogy and Petrology 68, 63–78.

Dyjor, S., 1993. Etapy blokowego rozwoju Sudetów i ich przedpola w neogenie i starszym czwartorzędzie. Folia Quaternaria 64, 25–41.

Dyjor, S., 1995. Young Quaternary and recent crustal movements in Lower Silesia, SW Poland. Folia Quaternaria 66, 51–58.

Dyjor, S., Oberc, J., 1983. Współczesne ruchy skorupy ziemskiej w Polsce SW i wynikające z nich możliwości zagrożeń dla obiektów górniczych i inżynierskich. III Kraj. Symp. "Współczesne i neotektoniczne ruchy skorupy ziemskiej w Polsce" IV. Ossolineum, Wrocław, pp. 7–23.

Frejková, L., 1968. Žáruvzdorné jíly u Uhelné u Javorníka ve Slezsku. Časopis pro mineralogii a geologii 13, 167–173.

French, H.M., 2007. The Periglacial Environment3rd Edition. J. Willey & Sons. 458 pp.

Gabriel, M., Gabrielová, N., Hokr, Z., Knobloch, E., Kvaček, Z., 1982. Miocén ve vrtu Vidnava Z-1. Sborník Geologických Věd, Geologie 36, 115–137.

Guterch, B., Lewandowska-Marciniak, H., 2002. Seismicity and seismic hazard in Poland. Folia Quaternaria 73, 85–99.

Ivan, A., 1997. Topography of the Marginal Sudetic Fault in the Rychlebské hory Mts. and geomorphological aspects of epiplatform orogenesis in the NE part of the Bohemian Massif. Moravian Geographical Reports 1 (5), 3–17.

Jarosiński, M., 2005. Ongoing tectonic reactivation of the Outer Carpathians and its impact on the foreland: results of borehole breakout measurements in Poland. Tectonophysics 410, 189–216.

Jarosiński, M., 2006. Recent tectonic stress field investigations in Poland: a state of the art. Geological Quarterly 50 (3), 303–321.

Kárník, V., Michal, E., Molnár, A., 1958. Erdbebenkatalog der Tschechoslowakei bis zum Jahre 1956. Geofysikální Sborník 69, 411–598.

Kontny, B., 2003. Geodezyjne badania współczesnej kinematyki głównych struktur tektonicznych polskich Sudetów i bloku przedsudeckiego na podstawie pomiarów GPS. Geodetic Research of Contemporary Kinematics of the Main Tectonic Structures of the Polish Sudetes and the Fore–Sudetic Block with the Use of GPS Measurements. Zesz. Nauk. AR we Wrocławiu 468, Wydz: Inżynierii, Kształtowania Środowiska i Geodezji, Rozprawy, vol. 202, pp. 1–146.

Kontny, B., 2004. Is the Sudetic Marginal Fault still active? Results of the GPS monitoring 1996–2002. Acta Geodynamica et Geomaterialia 1 (3 (135)), 35–39.

Krzyszkowski, D., Bowman, D., 1997. Neotectonic deformation of Pleistocene deposits along the Sudetic Marginal Fault, southwestern Poland. Earth Surface Processes and Landforms 22, 545–562.

Krzyszkowski, D., Migoń, P., Sroka, W., 1995. Neotectonic Quaternary history of the Sudetic Marginal Fault, SW Poland. Folia Quaternaria 66, 73–98.

Krzyszkowski, D., Pijet, E., 1993. Morphological effects of Pleistocene fault activity in the Sowie Mts., southwestern Poland. Zeitschrift für Geomorphologie, N. F., Supplement-Band 94, 243–259.

Krzyszkowski, B., Przybylski, D., Badura, J., 2000. The role of neotectonics and glaciation on terrace formation along the Nysa Kłodzka River in the Sudeten Mountains (southwestern Poland). Geomorphology 33, 149–166.

Křibek, B., Sýkorová, I., Machovič, V., Laufek, F., 2008. Graphitization of organic matter and fluid-deposited graphite in Palaeoproterozoic (Birimian) black shales of the Kaya-Goren greenstone belt (Burkina Faso, West Africa). Journal of Metamorphic Geology 26, 937–958.

Kwiecinska, B., Petersen, H.I., 2004. Graphite, semi-graphite, natural coke, and natural char classification — ICCP system. International Journal of Coal Geology 57, 99–116.

Lister, G.S., Snoke, A.W., 1984. S–C mylonites. Journal of Structural Geology 6, 617–638.

Loke, M.H., Barker, R.D., 1995. Least-squares deconvolution of apparent resistivity pseudosections. Geophysics 60, 1682–1690.

Mastalerz, K., Wojewoda, J., 1993. Alluvial-fan sedimentation along an active strike-slip fault: Plio-Pleistocene Pre-Kaczawa fan, SW Poland. Special Publication of the International Association of Sedimentologists 17, 293–304.

Matsuoka, N., 2001. Solifluction rates, processes and landforms: a global review. Earth-Science Reviews 55, 107–134.

McCalpin, J. (Ed.), 2009. Paleoseismology, Second Edition. Academic Press. 613 pp.

Migoń, P., 1993. Geomorphological characteristics of mature fault-generated range fronts, Sudetes Mts., Southwestern Poland. Zeitschrift für Geomorphologie, N. F., Supplement-Band 94, 223–241.

Mohammadioun, G. (Ed.), 1995. Proceedings of the Second France–United States Workshop on Earthquake Hazard Assessment in Intraplate Regions: Central and Eastern United States and Western Europe. October 16, 1995, Nice, France, Quest Éditions. Presses Académiques. 142 pp.

Moreno, X., Masana, E., Gràcia, E., Pallàs, R., Ruano, P., Coll, M., Štěpančíková, P., Santanach, P., 2007. Primeras evidencias de paleoterremotos en la falla de Carboneras: estudio paleosismológico en el segmento de La Serrata. Geogaceta 41, 135–138.

Nováková, L., 2009. Brittle Tectonic Investigations in the North-eastern Part of the Bohemian Massif, Czech Republic. 71st EAGE Annual Conference & Exhibition in Amsterdam 2009, Abstract, 6183.

Nováková, L., Schenk, V., 2008. Recent tectonic movements in the NE part of the Bohemian Massif, Czech Republic, indicated by the brittle tectonic approach. Geophysical Research Abstracts 10 EGU 2008-A-07801, poster.

Oberc, J., 1977. The Late Alpine Epoch in south-west Poland. In: Pozarski, W. (Ed.), Geology of Poland: Tectonics, vol. IV. Wydawnictwo Geologiscne, Warszawa, pp. 451–475.

Oberc, J., Dyjor, S., 1969. Uskok sudecki brzeżny. Biuletyn Institutu Geologicznego 236, 41–142.

Olczak, T., 1962. Seismiczność Polski w okresie 1901–1950. Acta Geophysica Polonica 10, 3–11.

Ondra, P., 1968. Zpráva o vrtném průzkumu miocenní pánve u Uhelné ve Slezsku. Zprávy o geologickém výzkumu v roce 1966, 266–267.

Pagaczewski, J., 1972. Catalogue of Earthquakes in Poland in 1000–1970 years: Mat. I Prace Inst. Geofiz., vol. 51. 36 pp.

Pecina, V., Čurda, J., Hanáček, M., Kočandrle, J., Nývlt, D., Opletal, M., Skácelová, D., Skácelová, Z., Večeřa, J., Žáček, V., 2005. Základní geologická mapa České republiky 1 : 25 000 s Vysvětlivkami 14-221 Žulová. Unpublished map, Czech Geological Survey, Praha.

Petley, D.N., 1998. Geomorphological mapping for hazard assessment in a neotectonic terrain. The Geographical Journal 64, 183–201.

Pouba, Z., Mísař, Z., 1961. O vlivu příčných zlomů na geologickou stavbu Hrubého Jeseníku. Časopis mineralogie a petrologie 6, 316–324.

Prosová, M., 1981. Oscilační zóna kontinentálního ledovce. Jesenická oblast. Acta Universitatis Carolinae-Geologica 25, 265–294.

Reimer, P.J., Baillie, M.G.L., Bard, E., Bayliss, A., Beck, J.W.J., Bertrand, C.J.H., Blackwell, P.G., Buck, C.E., Burr, G.S., Cutler, K.B., Damon, P.E., Edwards, R.L., Fairbanks, R.G., Friedrich, M., Guilderson, T.P., Hogg, A.G., Hughen, K.A., Kromer, B., McCormac, G., Manning, S., Bronk Ramsey, C., Reimer, R.W., Remmele, S., Southon, J.R., Stuiver, M., Talamo, S., Taylor, F.W., van der Plicht, J., Weyhenmeyer, C.E., 2004. INTCAL04 terrestrial radiocarbon age calibration, 0–26 cal kyr BP. Radiocarbon 46, 1029–1058.

Sikorová, J., Víšek, J., Nývlt, D., 2006. Texture and petrography of glacial deposits in the northern foothill of the Hrubý Jeseník and Rychlebské Mts., Czechia. Geological Quarterly 50, 345–352.

Skácel, J., 1978. Závěrečná zpráva o geologickém mapování na listu mapy 1:50.000 M-33-71-A Jeseník. Geologický průzkum – Ostrava. 165 pp.

Skácel, J., 1989. Křížení okrajového zlomu lugika a nýznerovského dislokačního pásma mezi Vápennou a Javorníkem ve Slezsku. Acta Universitatis Palackianae Olomucensis. Facultas Rerum Naturalium: Geographica-Geologica 28 (95), 31–45.

Skácel, J., 2004. The Sudetic Marginal Fault between Bílá Voda nad Lipová Lázně. Acta Geodynamica et Geomaterialia 3 (135), 31–33.

Suchý, V., Sýkorová, I., Melka, K., Filip, J., Machovič, V., 2007. Illite "crystallinity" coalification of organic matter and microstructural development associated with lowest-grade metamorphism of Neoproterozoic sediments in the Teplá-Barrandian unit, Czech Republic. Clay Minerals 42, 415–438.

Štěpančíková, P., Hók, J., 2009. Tectonic Hazard and Paleoseismological Research within the Sudetic Marginal Fault Zone (NE Bohemian Massif, Czech Republic). Proceedings of 17. Tagung für Ingenieurgeologie mit Forum für junge Ingenieurgeologen/17th Conference on Engineering Geology with Forum for Young Engineering Geologists, 6.–9. May 2009, Zittau, Germany, pp. 439–441.

Štěpančíková, P., Hók, J., Nývlt, D., Dohnal, J., Sýkorová, I., Stemberk, J., 2009. Active Tectonics within Sudetic Marginal Fault Zone (NE Bohemian Massif). 7th Meeting of the Central European Tectonic Studies Group (CETeG), 14th Meeting of the Czech Tectonic Studies Group (ČTS), HUNTEK 2009, 13–16 May 2009, Pécs, Hungary, p. 31.

Štěpančíková, P., Stemberk, J., Vilímek, V., Košťák, B., 2008. Neotectonic development of drainage networks in the East Sudeten Mountains and monitoring of recent fault displacements (Czech Republic). Special Issue on: Impact of Active Tectonics and Uplift on Fluvial Landscapes and River Valley Development. Geomorphology 102, 68–80.

Tuinistra, F., Koenig, J.L., 1970. Raman spectrum of graphite. Journal of Chemical Physics 53, 1126–1130.

Wells, D.L., Coppersmith, K.J., 1994. Empirical relationships among magnitude, rupture length, rupture area, and surface displacement. Bulletin of the Seismological Society of America 82, 974–1002.

Žáček, V., et al., 1995. Geologická mapa ČR, 1:50 000, 14–22 Jeseník. Czech Geological Survey, Praha.

Zuchiewicz, W., Badura, J., Jarosiński, M., 2007. Neotectonics of Poland: an overview of active faulting. Studia Quaternaria 24, 5–20.